Spectroscopic evidence for the direct involvement of local moments in the pairing process of the heavy-fermion superconductor math xmlns="http://www.w3.org/1998/Math/MathML">msub>mi>CeCoIn/mi>mn>5/mn>/msub>/math>

K. Shrestha, S. Zhang, L. H. Greene, Y. Lai, R. E. Baumbach, K. Sasmal, M. B. Maple, and W. K. Park

Phys. Rev. B **103**, 224515 — Published 10 June 2021

DOI: 10.1103/PhysRevB.103.224515

Spectroscopic Evidence for the Direct Involvement of Local Moments in the Pairing Process of the Heavy-Fermion Superconductor $CeCoIn_5$

K. Shrestha[1,†], S. Zhang[1, 2], L. H. Greene[1, 2], Y. Lai[1,2], R. E. Baumbach[1,2], K. Sasmal[3], M. B. Maple[3], and W. K. Park[1,*]

[1]*National High Magnetic Field Laboratory, Florida State University, Florida, 32310, USA*
[2]*Department of Physics, Florida State University, Florida, 32306, USA*
[3]*Department of Physics, University of California, San Diego, California, 92093, USA*

Abstract

The microscopic mechanism for electron pairing in heavy-fermion superconductors remains a major challenge in quantum materials. Some form of magnetic mediation is widely accepted with spin fluctuations as a prime candidate. A novel mechanism, "composite pairing" based on the cooperative two-channel Kondo effect directly involving the *f*-electron moments has also been proposed for some heavy fermion compounds including $CeCoIn_5$. The origin of the spin resonance peak observed in neutron scattering measurements on $CeCoIn_5$ is still controversial and the corresponding hump-dip structure in the tunneling conductance is missing. This is in contrast to the cuprate and Fe-based high-temperature superconductors, where both characteristic signatures are observed, indicating spin fluctuations are likely involved in the pairing process. Here, we report results from planar tunneling spectroscopy along three major crystallographic orientations of $CeCoIn_5$ over wide ranges of temperature and magnetic field. The pairing gap opens at $T_p \sim 5$ K, well above the bulk $T_c = 2.3$ K, and its directional dependence is consistent with d_{x2-y2} symmetry. With increasing magnetic field, this pairing gap is suppressed as expected but, intriguingly, a new gaplike structure emerges smoothly, increasing linearly up to the highest field applied. This field-induced gaplike feature is only observed below T_p. The concomitant appearance of the pairing gap and the field-induced gaplike feature, along with its linear increase with field, indicates that the *f*-electron local moments are directly involved in the pairing process in $CeCoIn_5$.

[†] Present address: Department of Chemistry and Physics, West Texas A&M University, 2501 4th Ave, Canyon, Texas 79016, USA.

[*] To whom correspondence should be addressed. Email: wkpark@magnet.fsu.edu.

I. INTRODUCTION

The unconventional heavy-fermion superconductor $CeCoIn_5$ has the critical temperature (T_c) of 2.3 K and a d_{x2-y2} superconducting (SC) order parameter symmetry [1,2]. Since its discovery, the glue for electron pairing has been suggested to entail magnetic mediation, but the precise mechanism remains to be revealed. In the cuprate and Fe-based high-temperature superconductors (HTS) [3], antiferromagnetic spin fluctuations [4-6] have been identified as playing a major role in the Cooper pairing based on the observation of the neutron spin resonance and the corresponding signature in tunneling conductance [7-11], which is how the phonon-mediated pairing mechanism was confirmed in conventional superconductors [12-15]. This is not the case for $CeCoIn_5$ as the origin of the neutron resonance peak at Ω_{res} = 0.6 meV remains controversial [16-18], and there is no corresponding feature in the tunneling data [19-23], suggesting a different pairing interaction. The anomalous magnetic susceptibility in $CeCoIn_5$, which indicates the presence of un(der)-screened moments [24] down to T_c, led Coleman and co-workers to propose a new pairing mechanism [25,26] in which "composite" pairs are formed between local moments and conduction electrons through a cooperative two-channel Kondo effect [27-29].

Here we report results from planar tunneling spectroscopy (PTS) [30] measurements on $CeCoIn_5$. In addition to the main SC phase with d_{x2-y2} symmetry in $CeCoIn_5$, there exists another distinct phase, the Q-phase (previously thought to be the Fulde-Ferrell-Larkin-Ovchinnikov phase [31-33]), appearing only in a limited region of the phase diagram (low temperature and high magnetic field) [34-36]. In this paper, we focus our discussion on the overall temperature and field dependences since no noticeable changes are observed in the Q-phase. Our detailed and reproducible tunneling conductance spectra provide strong evidence for: i) the existence of preformed pairs well above T_c; and ii) the direct involvement of localized *f*-electron moments in the pairing process. Surprisingly, local physics manifested via Kondo resonance appears to play a key role in the superconductivity in this compound.

II. EXPERIMENTS

The $CeCoIn_5$ single crystals used in our studies were grown by three independent groups using the flux method [37]. High-quality crystals, based on both magnetization and resistivity measurements, were chosen and cut to have the surface orientation along three major crystallographic axes, namely, [001], [100], and [110], as determined by single crystal x-ray diffraction [38]. They were fixed on epoxy (Stycast® 2850-FT) molds and then polished down to 1.0 – 1.5 nm peak-to-dip smoothness (Fig. S1 in [39]). The superconductor/insulator/superconductor (S-I-S') tunnel junctions were prepared by depositing a 2.0 – 2.5 nm-thick aluminum layer on the polished crystal surface, followed by subsequent plasma oxidation, then deposition of lead (Pb) strips as counter electrodes (Fig. S2 in [39]).

Measurements of the differential tunneling conductance across the junction, $G(V) \equiv \frac{dI}{dV}$, were carried out using the four-probe lock-in technique over wide ranges of temperature (T, down to 20 mK) and magnetic field (H, up to 18 T). Here, V is 'Sample Bias' voltage applied to the $CeCoIn_5$. Only the conductance spectra from high-quality junctions, determined by the sharpness of the Pb coherence peaks and phonon features (Figs. S3 – S5 in [39]), are reported here. The conductance spectra of $CeCoIn_5$, as presented in the main text, were obtained by driving the Pb normal with a small magnetic field (H = 0.2 T). Unless otherwise specified throughout this paper, magnetic fields were applied perpendicular to the junction plane. We define the normalized conductance in two different ways: i) $G_n(V) \equiv G(V)/G(-V_{max})$, where $-V_{max}$ is the negative maximum bias voltage; ii) $G_b(V) \equiv G(V)/G_{bg}(V)$, where the background conductance $G_{bg}(V)$ is obtained from a polynomial fitting of the G(V) in the high-bias region. The typical junction resistance was R_J = (20 – 50) Ω, and the product $R_J \cdot A$ = was 10-20 Ωmm^2, where A is the junction area. See Supplemental Material ([39] Sect. 1. Materials and Methods) for additional details.

III. SUPERCONDUCTING ORDER PARAMETER AND PRE-FORMED PAIRS

The tunneling conductance data taken at 20 mK are plotted in Fig. 1. While both (001) and (100) junctions show sharp coherence peaks, the (110) junction exhibits a pronounced zero-bias conductance peak (ZBCP). To extract the SC gap, Δ, the $G_b(V)$ curves from the (001) and (100) junctions are analyzed by fitting to the *d*-wave Blonder-Tinkham-Klapwijk (BTK) model [40,41] with three adjustable parameters: Δ, Γ, and Z (Sect. 2 in [39]). Here, Γ is the quasiparticle lifetime broadening parameter and Z represents the dimensionless barrier strength. Unlike the (100) junction in Fig. 1(b), the U-shape subgap-conductance of the (001) junction can't be replicated by the d-wave BTK model as seen in Fig. 1(a), possibly due to the tunneling cone effect (Fig. S6 in [39]). The extracted Δ value is 0.66 meV and 0.54 meV for the [001] and [100] directions, respectively, falling in the range reported in the literature [1,19-23]. The ZBCP seen in the (110) junction can be a characteristic feature of a nodal junction on a *d*-wave superconductor, arising from surface bound states formed due to the sign-changing nature of the *d*-wave order parameter, known as Andreev bound states (ABS) [42-45]. Thus, overall, the anisotropy in our tunneling conductance agrees with the well-established d_{x2-y2}–wave pairing symmetry in $CeCoIn_5$ [1,2]. On a closer look, the ZBCP consists of two structures: A wider peak of Lorentzian shape as shown by the red solid line and a narrower peak sitting on top of the former. The wider peak itself is not due to ABS, as discussed later regarding its magnetic field dependence. The narrower structure can be seen more clearly in the left inset of Fig. 1(c), plotting the $G_b(V)$ further normalized by the Lorentzian background [46]. It consists of slightly split peaks, reminiscent of the Doppler shift of ABS under a magnetic field (0.2 T) [47,48]. The gap edge expected to be seen along with the ZBCP is not apparent presumably because the peak isn't narrow enough compared to the small Δ in $CeCoIn_5$. The detailed behavior of this possibly ABS-originated ZBCP remains to be further investigated.

Figure 2 shows temperature evolution of the tunneling conductance along the three directions in both waterfall plots, (a) – (c), and color contour maps, (d) – (f). For a (001) junction in Fig. 2(a), with decreasing temperature, a broad ZBCP emerges and gradually grows until $T_p \sim 5$ K, where it begins to split, as shown more clearly in the left inset, smoothly evolving into a SC gap that turns into well-defined coherence peaks at low temperature. Thus, we interpret the splitting of the ZBCP as due to the opening of a gap in the single particle spectrum caused by the pairing of conduction electrons. The right inset displays the ZBC vs. T, which shows a sharp drop at $T \sim 5$ K, further confirming the temperature scale, $T_p \sim 5$ K. The pairing gap persisting above T_c can also be seen in the color-contour map in Fig. 2(d). This is in agreement with previous scanning tunneling spectroscopy (STS) [19,20], resistivity [49], and thermal conductivity [50] studies that identified a pseudogap in this temperature range. Four-fold oscillations in the field-angle dependent thermal conductivity [50], an evidence for the d_{x2-y2} pairing symmetry in $CeCoIn_5$, were observed up to $T = 3.2$ K, implying that the pairing gap above T_c has the same symmetry as that below T_c. The persistence of the Curie-Weiss temperature dependence of the DC magnetic susceptibility, χ, another bulk property, down to just above T_c was one of the key experimental observations underlying the theoretical proposal for a novel pairing mechanism in $CeCoIn_5$ [25,26]. On a close look, we notice that χ exhibits a slight but clear slope decrease below $\sim T_p$ in its Curie-Weiss plot vs. $1/T$ (Fig. S7 in [39]). As χ in $CeCoIn_5$ is primarily due to the Ce^{3+} ions or localized $4f^1$ electrons, this slope decrease concomitant with the opening of the pairing gap as seen in our tunneling spectroscopy suggests that, indeed, the Ce-4f electrons might be directly involved in the pairing process [25,26]. The pairing gap above T_c in $CeCoIn_5$ is reminiscent of the pseudogap in high-T_c cuprates [51,52]. And, the continuous evolution of the pairing gap feature crossing the T_c implies that preformed pairs exist in the pseudogap region below T_p, whose nature is further discussed later.

In the above discussion, we have shown that the onset of the pairing gap at $T_p > T_c$ evidenced in our single electron tunneling spectra is also consistent with other bulk properties including resistivity, thermal conductivity, and magnetic susceptibility. On the other hand, there is no such evidence in the specific heat (C) [24] or Andreev reflection (AR) measurements [1]. This can be understood as follows. Since $C = -T\frac{\partial^2 F}{\partial T^2}$, where F is the free energy, it is directly tied to the SC order parameter, $\Psi_{SC} = |\Psi|e^{i\varphi}$, where φ is the phase factor. Preformed pairs in the pseudogap region are not yet condensed into the same ground state, so $\Psi_{SC} = 0$, hence there would be no signature in C across T_p. In the case of AR, if an electron of energy E from the normal metal is injected into the superconductor, the phase change during its reflection as a hole is given by $\Phi = \varphi + \cos^{-1}(E/\Delta)$. It is generally believed that the AR conductance is detectable because the superconductor has a well-defined order parameter with a definite φ. Thus, the reason why the AR conductance is zero in the preformed pair state of $CeCoIn_5$ [1] could be because φ is random among the pairs, that is, they remain incoherent down to T_c. It is an open question whether AR can still occur off individual pairs [53] but incoherently, resulting in overall cancellation in typical time-averaged measurements such as differential conductance or it can't occur at all until full phase coherence is reached below T_c.

Figures 2(b) & 2(e) show the temperature evolution of $G_b(V)$ for a (100) junction. The pairing gap feature persists above T_c albeit weaker, similarly to that of the (001) junction in Fig. 2(a). This is also evidenced by the drop of the ZBC below ~ 4 K, as shown in the inset of Fig. 2(b). It is notable that the pairing gap feature in this junction emerges out of a zero-bias conductance dip (ZBCD), in contrast to the gap emerging out of a ZBCP in the (001) junction (Fig. 2(a)). Empirically, (001) junctions have been observed to show a ZBCP more frequently than a ZBCD, whereas it is opposite for (100) junctions. (110) junctions always exhibit a ZBCP. While further investigations are necessary to pin down the exact origin for these discrepant behaviors, here we discuss some clues. In a Kondo system (whether single impurity or lattice), electrons can co-tunnel into the conduction band and the localized state (orbital) [54-57], resulting in a Fano resonance with the conductance shape strongly depending on the Fano parameter, q_F [54,58]. Thus, the variation of the conductance shape can be attributed to the q_F value: A peak (dip) for large (small) q_F due to the predominant tunneling into the localized orbital (conduction band) in these junctions (Fig. S8 in [39]). Related to this, we note the ZBC has a finite value even at very low temperatures in both the (001) and (100) junctions, as shown in Fig. 1. Our smallest observed ZBC is 19% (not shown) of the high-bias conductance, substantially smaller than that (~50%) reported in most of the previous STS measurements [19,21-23]. A finite conductance within the SC gap at such a low temperature cannot be explained by the thermal population effect alone. Based on our observation of both ZBCP and ZBCD as mentioned above (e.g., see Fig. S9 in [39]), we speculate that it may be associated with the existence of non-trivial tunneling channels, an intrinsic property of $CeCoIn_5$, as detailed below. The temperature evolution of a (110) junction is shown in Figs. 2(c) & 2(f) from 0.4 K up to 30 K (see Fig. S10 in [39] for another set of conductance spectra). The ZBCP becomes wider with increasing temperature with the ZBC showing a logarithmic dependence in the intermediate temperature range, reminiscent of a Kondo resonance. The persistent observation of a ZBCP in all (110) junctions suggests that the Kondo resonant tunneling off the localized Ce $4f^1$ moments is enhanced in this direction compared to other directions. This is in agreement with a recent report [59] that the lobe direction of the ground state $4f$ orbital in $CeCoIn_5$ is [110]. The ZBCPs observed in some non-nodal junctions (e.g., Fig. S11 in [39]) may have a similar origin, presumably caused by the crystal surface' atomic-scale structure being favorable for a Kondo resonant tunneling, i.e., along the $4f$ orbital's lobe direction. Within this local picture, the ZBCDs observed in the other non-nodal junctions can also be understood as due to a dominant tunneling along the 4*f* orbital's nodal direction, namely, into the conduction band, resulting in a ZBCD due to an anti-resonance.

To determine the temperature dependence of Δ, we have analyzed the conductance data displayed in Fig. 3(a), which were taken from a (001) junction. For simplicity, $G_b(V)$ is obtained by dividing out G(V) at each temperature with G(V) at 5 K that shows a ZBCD, which is then fit to the *d*-wave BTK model [40,41]. Best fits are obtained with Z kept to a constant value of 5.0, well in the tunneling limit, and plotted in Fig. 3(b). The temperature dependence of extracted Δ and Γ is shown in Fig. 3(c). At $T = 0.4$ K, $\Delta = 0.87$ meV, again falling in the range reported in the literature [1,19-23]. Note Δ decreases gradually with *T*, has a finite value above T_c, and tends to zero only at $T \sim 5$ K (dashed line). Meanwhile, Γ increases with *T*, as expected. It is notable that at T_c, $\Delta \sim 3\Gamma$ within the error bar. A similar scaling behavior between Δ and Γ has been reported in photoemission studies of some high-T_c cuprates [60] and can also be seen in an STS study of $CeCoIn_5$ [20]. Assuming that Γ is related to a pair-breaking scattering rate, $\Gamma = \hbar/\tau$, where τ is the lifetime of the Cooper pair, this result can be interpreted as follows: with decreasing temperature below $T_{p,}$ the density of Cooper pairs increases until a critical density is reached and condensation occurs [60]. Thus, the relationship $3\Gamma(T)/\Delta(T)|_{T=Tc} = 1$ appears to define T_c. However, it should be noted that not all junctions show exactly the same scaling behavior as in this junction. A more in-depth analysis is required to address whether this is due to the tunneling spectrum being affected by the Kondo (anti-)resonance, as discussed above.

IV. ANOMALOUS EVOLUTION OF THE PAIRING GAP UNDER MAGNETIC FIELD

The magnetic field evolution of the tunneling conductance is shown in Fig. 4 for all three directions. For the (001) and (100) junctions, the application of an external magnetic field suppresses the pairing gap feature gradually, as expected, but an intriguing field-induced gaplike feature (FIG) emerges at higher fields. We stress that the FIG appears even before the closing of the pairing gap at the upper critical field ($H_{c2} = 4.95$ T and 11.8 T along the [001] and [100] directions, respectively) [31]. Note that both the depth and width of the FIG increase with increasing field up to 18 T, the highest field applied. Note also that the FIG is observed below T_c (Figs. 4(a)-(b)) and above T_c (Figs. 4(d)-(e)). In both orientations, the tunneling conductance shows a crossover from the SC gap feature to the FIG. In contrast, the nodal junction exhibits a ZBCP both below and above T_c with no apparent pairing gap, as already seen in Figs. 1 & 2. At $T = 20$ mK, the top part of the ZBCP is split at $H = 0.2$ T, which could be a signature for the Doppler shift of ABS as discussed in Fig. 1(c). However, the major part of the ZBCP can't be a signature for ABS since it splits persistently all the way up to 18 T, well above H_{c2}. Instead, it may originate from a Kondo resonance, as mentioned earlier, a part of the hybridization process leading to the lattice coherence. Indeed, the sharp

ZBCP at low temperature is seen to grow out of a broad ZBCP that begins to appear below 45 K (see Fig. S10 in [39]), widely known as the coherence temperature in $CeCoIn_5$ [24]. At T = 5 K, the splitting is not observed until $H \approx 14$ T, whose exact understanding beyond the thermal population effect requires further investigations since the splitting must be intimately tied to the exact origin of the ZBCP.

Prior to conducting a quantitative analysis of the field dependence just described above, it is important to determine whether the FIG is due to an extrinsic or intrinsic effect, and if intrinsic, whether it reflects the surface or bulk property. Based on the data shown in Fig. 4, three possibilities can be considered (see Fig. S2(c) in [39]): case A – extrinsic magnetic moments in the barrier or at the interface; case B – surface Ce^{3+} ions acting as Kondo impurities; case C – bulk effect. A magnetic moment in the tunnel barrier or at the interface can cause a (Kondo) resonant tunneling at the Fermi level, showing up as a ZBCP, and an applied magnetic field causes a Zeeman splitting, as observed frequently in PTS and STS [61-63] and explained by the Anderson-Appelbaum (AA) theory [64,65]. The ZBCP observed in the nodal junction on $CeCoIn_5$ and its splitting under an applied magnetic field is reminiscent of this single impurity Kondo effect. However, such a ZBCP has never been observed in our junctions prepared on many other materials than $CeCoIn_5$ using the same procedure to form AlO_x [66] and is extremely rarely reported in the literature [61], albeit the possibility of forming magnetic moments in AlO_x [67]. The FIG in $CeCoIn_5$ has also been reported in recent STS studies [21,23], in which tunneling conductance was measured on a surface cleaved freshly in vacuum, so such magnetic moments of extrinsic origin can be ruled out. Thus, we are left with the other two possibilities for the intrinsic origin of the FIG. For case B, a metallic point-contact junction on $CeCoIn_5$ is expected to exhibit a ZBCD but such a signature due to single impurity Kondo scattering [68] has never been observed in our measurements on all three surfaces of $CeCoIn_5$ [1,69]. In addition, our analysis of the ZBCP using the Frota function [46] and its temperature evolution in terms of interaction-induced broadening within the strong coupling regime [63,70] (see Fig. S13 in [39]) suggests that case C is more likely than case B. Thus, we conclude the FIG reflects a bulk property of $CeCoIn_5$.

For further analysis of the FIG, in Figs. 4(g) – (i), we plot the low-temperature field evolution of the nominal peak position, V_p, corresponding to the SC gap at low fields and the FIG at high fields. For the (001) and (100) junctions, V_p decreases gradually as expected for a pairing gap, but only up to the crossover field, $H_{cr} \approx 4.0$ T, above which it increases linearly due to the FIG's takeover. This crossover behavior is also seen in the field dependence of the ZBC (Fig. S12 in [39]). It is interesting that, although the FIG is dominant above H_{cr}, the pairing gap along [100] is seen to persist up to H_{c2} (Fig. S14 in [39]), as shown by V_{ps} in Fig. 4(h) at which the conductance slope change is clearly observed. If the V_p below H_{cr} is extrapolated to the field axis using the field dependence of the pairing gap given by the Ginzburg-Landau (GL) theory [71], $\Delta(H) = \Delta(0)\sqrt{1-(H/H_{c2})^2}$, where $\Delta(0)$ is the gap at zero field, $V_p = 0$ at $H \approx H_{c2}$ in both directions. This confirms that the pairing gap observed in our PTS represents a bulk property. Unlike the (001) and (100) junctions, V_p in the nodal junction increases linearly up to the highest field applied.

The nominal peak position (V_p) increases linearly above H_{cr} in the non-nodal and at all fields in the nodal junctions and, extrapolating from high field, (H, V_p) approaches (0, 0) (green dash-dotted lines). The (001) junction shows a slight offset when extrapolated to zero field. This may be explained by the large smearing effect (Γ) in this junction, which can be inferred from the larger Γ/Δ ratio at zero field compared to the (100) junction (see the Fig. 4 caption). The linear increase of the field-induced splitting is reminiscent of the Zeeman effect: $eV_p = E_Z = \frac{1}{2} g\mu_B H$, where E_Z is the Zeeman energy, g is the Landé g-factor, and μ_B is the Bohr magneton. However, it is well known that, for tunneling into single Kondo impurities [61-63], the slope of a V_p vs. H plot gives a wrong g-value. Instead, the g-factor can be determined reasonably accurately by taking the point where the slope of the conductance is largest, V_s. This is also justified from our simulation (see Fig. S15(a) in [39]), so we determine V_s as a function of the field (Fig. S15(b) in [39]). The V_s values are plotted in Figs. 4(g) – 4(i), in which (H, V_s) extrapolates to (0, 0) for all three junctions (see black dashed lines). Since V_s is determined more rigorously than V_p as mentioned above, this common behavior of V_s must reflect an intrinsic property of the FIG. From the linear fit of the V_s vs. H plot shown in Figs. 4(g) – 4(i), we deduce g values as follows: 1.81 ± 0.43, 2.14 ± 0.22, and 1.96 ± 0.25 for the [001], [100], and [110] directions, respectively. Thus, our g-factor is isotropic within error bars and in good agreement with the g-value of 1.92 determined from the field-induced splitting of the neutron spin-resonance peak [72]. From the analysis of the temperature dependence of H_{c2}, Won et al. [73] reported an anisotropic g-factor: 1.5 for [001] and 0.62 for [100]. In a Pauli-limited superconductor, the critical field [74] is given by $H_P = \sqrt{2}\Delta(0)/g\mu_B$, where $\Delta(0)$ is the SC gap at H = 0. Using our Δ and g values, we estimate H_P = 8.9 – 11.7 T, 6.2 T, and 6.7 T for [001], [100], and [110] directions, respectively. Note that the in-plane H_P values are much smaller than the measured upper critical field, H_{c2} = 11.8 T [31], warranting a revisit to the widely accepted Pauli-limited nature of the pairing in $CeCoIn_5$.

V. DIRECT INVOLVEMENT OF LOCAL MOMENTS IN THE PAIRING PROCESS

The FIG in $CeCoIn_5$ is robust and reproducibly observed in multiple single crystals from different sources (Figs. S16, S17 in [39]) along all three crystallographic directions at $T < T_c$ and $T_c < T < T_p$, suggesting a common physical origin. Our conductance data on a (001) junction taken at two temperatures above T_p, namely, at T = 10 K and 15 K, are shown in Fig. 5. Here, with increasing field, the broad ZBCP is only suppressed gradually without showing a clear signature for the FIG up to 14 T, eventually merging into the background. This distinct behavior above T_p points to a concomitance of the pairing gap and the FIG, suggesting that the FIG is closely tied to the pairing mechanism. In addition, the FIG doesn't show any dependence on the field direction relative to the junction plane in all junctions (Fig. S18 in [39]). This is in line with the neutron spin resonance in $CeCoIn_5$ occurring at scattering wave vectors in three spatial dimensions [16].

As mentioned earlier, the compelling experimental fingerprint for spin fluctuation mediated pairing in the cuprate and Fe-based HTS is the spin resonance peak at $\omega = \Omega_{res}$ detected by inelastic neutron scattering , which also shows up in tunneling conductance as an additional dip-hump structure at $eV = \Delta + \Omega_{res}$ outside the coherence peaks [7-11] (Sect. 11 in [39]). The origin of the neutron resonance peak at $\Omega_{res} = 0.6$ meV in $CeCoIn_5$, despite the original interpretation as such a fingerprint [16], remains controversial [17,18], and the dip-hump structure is not observed in tunneling, neither in our PTS nor in the previous STS measurements [19-23]. Recently, van Dyke et al. [75] reproduced the neutron spin resonance peak by solving the SC gap equations and claimed the spin fluctuation mechanism in $CeCoIn_5$, but without accounting for the missing feature in tunneling conductance. It is clear that the pairing mechanism in $CeCoIn_5$ is yet to be determined. Below, we show that the signatures observed in our tunneling spectra are closely related to the pairing mechanism.

Coleman and coworkers [25,26] proposed a novel pairing mechanism based on the two-channel Kondo effect [27-29]. According to this theory, localized moments due to $4f^1$ electrons in $CeCoIn_5$ can be screened by conduction electrons via two channels. If this two-channel screening occurs cooperatively, the conduction electrons are effectively paired via the Kondo effect, leading to a composite pair. Here, the two-fold degeneracy of the crystal-field-split ground state Kramers doublet [59] is crucial, as it is for the single-channel Kondo effect. It is expected that, with the application of a magnetic field, the degeneracy is gradually lifted due to the Zeeman splitting, ultimately suppressing the composite pair formation. While a smoking gun evidence remains to be found, this exotic pairing has been invoked to explain the anomalous evolution of the gap structure observed in London penetration depth measurements on $Ce_{1-x}Yb_xCoIn_5$ [76,77].

As discussed earlier, our conductance spectra for non-nodal and nodal junctions exhibit distinct field evolutions. At low fields, the non-nodal junctions exhibit the pairing gap, whereas it is not seen in the nodal junction. This may be accounted for as being due to the sign-change of the d_{x2-y2} -wave order parameter, causing pairs to be broken on the nodal surface, as is well known for the high-T_c cuprates [42-45]. However, stronger evidence for ABS in $CeCoIn_5$ is yet to be found since its characteristic signatures seem to appear on top of much stronger background, namely, a Kondo resonance over an energy scale comparable to Δ, as mentioned earlier. This suggests that $CeCoIn_5$ may possess a more complex SC order parameter than a simple *d*-wave form. If the ZBCP arises from Kondo resonant tunneling, it would split under magnetic fields due to the Zeeman splitting of the Ce $4f^1$ moment. This is supported by fact that the ZBCP begins to split at low fields in the absence of an apparent pairing gap. For non-nodal junctions, the FIG appears to be masked by the pairing gap until the field becomes strong enough to break a large portion of the pairs. These unpaired electrons can then participate in resonant and inelastic tunneling involving the localized moment [64,65], which is consistent with the V_p undergoing a crossover at H_{cr}. Toward a more microscopic understanding of the crossover, two characteristic energy scales instead of nominal bias voltages should be compared, namely, Δ and E_Z. By solving the equation, $\Delta(H) = \Delta(0)\sqrt{1-(H/H_{c2})^2} = 1/2g\mu_B H$, and using our extracted values for $\Delta(0)$ and g along with the known H_{c2}, we obtain the crossing field, $H_c \sim 4.6$ T and 7.0 T for the (001) and (100) junctions, respectively, as marked by the gray line in Figs. 4(g) and 4(h). Notably, H_c is anisotropic, as is H_{c2} but unlike the isotropic H_{cr}, further supporting that the pairing mechanism and the FIG are intimately tied (as H_{c2} depends on the depairing mechanism, orbital or Pauli-limited). While the pairing gap signature in the (001) junction is missing for $H > H_{cr}$ due to the closeness of H_c to H_{c2} in this direction, it is seen to coexist with the FIG in the (100) junction in some field range above H_c since H_c is much smaller than H_{c2} in this direction (see Fig. S14 in [39]). At high temperature ($T > T_p \approx 5$ K), the pair formation might be suppressed presumably because increased thermal fluctuations weaken the cooperative effect between the two Kondo screening channels. Thus, the concomitance of the FIG with the pairing gap below T_p might be due to the Kondo resonance itself playing a key role in the pair formation.

In the high-field limit, the FIG is of qualitatively similar V-shape among the non-nodal junctions, whereas it exhibits quite a different structure in the nodal junction, as shown in Fig. 6(a) and 6(b), respectively. These curves are compared with computed ones based on the AA theory [62,64,65] shown in Fig. 6(c). As mentioned earlier, the tunneling conductance involving Kondo impurities has been qualitatively accounted for by this theory [61-63]. Here, the conductance frequently exhibits U-shape in the high-field limit. This is because both the spin-flip inelastic tunneling and the Kondo resonant tunneling, whose conductance contribution is denoted as G_2 and G_3, respectively, in the literature, give rises to a step-like abrupt increase at bias voltages corresponding to $\pm E_Z$. Apparently, this is not the case for our data since the computed curves don't resemble them at all. On a close look, there exist two linear regions within the FIG for the (110) junction and the boundary appears to be close to E_Z. We associate the discrepancy in the FIG observed in between our tunneling data and the computed curves with the non-trivial nature of the Kondo resonance, which, in turn, is tied to the nature of pairing. The cooperative two-channel Kondo effect, proposed to give rise to the pairing in $CeCoIn_5$, may lead to such unusual Kondo resonance. Also, we note that theoretically the same effect could explain the non-Fermi liquid behavior [27] clearly observed in this compound below ~20 K [24,49,78], coincident with the onset temperature for the ZBC's upturn, as seen in Fig. 2(c). For a full account of the FIG, it is desirable to formulate a more microscopic model that explains, both qualitatively and quantitatively, how the magnetic field suppresses such pairing that directly involves the localized f -moments. Such model would also take into account the exact ground state for the Ce $4f^1$ electron in $CeCoIn_5$ as it has been recently identified to be a Kramer's doublet, that is, $\Gamma_{7-} = \alpha|\pm5/2> + \beta|\mp3/2>$, arising from the crystal-electric field effect [59].

VI. CONCLUSION

In summary, our PTS data on $CeCoIn_5$ and analyses reveal the existence of preformed pairs at $T_p \sim 5$ K, well above $T_c = 2.3$ K, consistent with the previously reported STS and several bulk measurements. Upon lowering the temperature below T_p, both the density of pairs and their lifetime increase due to the reduction in thermal fluctuations, allowing them to condense into a phase coherent state at T_c. The pairing symmetry inferred from the directional dependence is d_{x2-y2}, in overall agreement with the literature, although its detailed nature is yet to be unraveled. With the application of a magnetic field, the pairing gap gradually turns into the FIG. And the FIG appears only at temperatures up to where the pairing gap persists. This concomitance of the pairing gap and the FIG provides a clue for the microscopic pairing mechanism in $CeCoIn_5$. The FIG exhibits linear field dependence and non-trivial structure, suggesting that the pairing in $CeCoIn_5$ may directly involve localized moments, e.g., via the cooperative two-channel Kondo effect that has been proposed theoretically.

ACKNOWLEDGEMENTS

We acknowledge fruitful discussions with A. V. Balatsky, A. V. Chubukov, P. Coleman, P. Ghaemi, J. D. Thompson, and K. Yang. The work at FSU (KS, SZ, LHG, and WKP) was supported by the US National Science Foundation (NSF), Division of Materials Research (DMR), under Award No. NSF/DMR-1704712. YL and RB acknowledge support from Department of Energy through the Center for Actinide Science (an EFRC funded under Award DE-SC0016568). A portion of this work was performed at the National High Magnetic Field Laboratory, which is supported by the NSF Cooperative Agreement No. NSF/DMR-1644779 and the State of Florida. The work at UCSD was supported by the US DOE-BES, DMSE, under Grant No. DEFG02-04-ER46105 (single crystal growth) and US NSF/DMR-1206553 (physical properties measurements).

FIGURE CAPTIONS

Fig. 1. Comparison of tunneling conductance along three major crystallographic directions of CeCoIn$_5$: (a) (001), (b) (100), and (c) (110). The temperature is 20 mK and the applied magnetic field is 0.2 T (Pb driven normal). Main panels show the normalized conductance, $G_b(V)$, obtained by dividing out the raw data with the (~ parabolic) background, as shown in the right insets. The lines in (a) & (b) are best fits to the *d*-wave BTK model, with fit parameters (Δ, Γ, Z) = (0.66 meV, 0.042 meV, 2.28) and (0.535 meV, 0.198 meV, 1.21), respectively, where Γ is the quasiparticle lifetime broadening parameter and Z represents the dimensionless barrier strength. The red solid line in (c) is a fit of the wider peak of Lorentzian shape to the Frota function depicting a Kondo resonance (Ref. 45): $G_{\mathrm{fit}}(V) = 0.985 + 0.18 \times Re\sqrt{\left(\frac{0.75\times10^{-3}i}{V+0.75\times10^{-3}i}\right)}$. The left inset is the conductance at low bias further normalized by the Frota fit background shown in the main panel.

Fig. 2. Temperature evolution of the background-normalized tunneling conductance in CeCoIn$_5$. The applied magnetic field is kept at 0.2 T. (a) – (c), waterfall plots of the conductance at varying temperature for (001), (100), and (110) junctions, respectively. Curves are shifted vertically in (a) and (b) for clarity. (d) – (f), corresponding color contour plots of the conductance with the y-axis (temperature) in logarithmic scale. The right insets show temperature dependence of the zero-bias conductance. In the left inset of (a), conductance curves around T_p (≈ 5 K) are plotted to show more clearly the evolution from a broad ZBCP to gaplike split peaks. The white horizontal dashed lines are to mark the bulk T_c (2.3 K).

Fig. 3. Opening of the pairing gap well above T_c in CeCoIn$_5$. (a) Temperature-dependent $G_n(V)$ for a (001) junction in which the pairing gap emerges out of a ZBCD below T_p instead of a ZBCP. The coherence peaks become sharp at low temperature. The curves overlap well at high bias. Inset: Magnified view of the gap edge. (b) $G_b(V)$ curves (black symbols) and their best fits (solid orange lines) to the d-wave BTK model. $G_b(V)$ is obtained by dividing out each $G_n(V)$ with $G_n(V)$ at 5 K. (c) Best-fit values for Δ and Γ. Z is kept to be a constant, 5. At 0.4 K, (Δ, Γ, Z) = (0.855 meV, 0.179 meV, 5.0). Δ remains finite above T_c and extrapolates to zero at T_p ~ 5 K, as indicated by the dashed line.

Fig. 4. Magnetic field evolution of the background-normalized conductance in CeCoIn$_5$. (a) – (c), waterfall plots of the conductance for varying magnetic field applied along the junction normal at temperatures well below T_c for (001), (100), and (110) junctions, respectively. (d) – (f), the same at temperatures well above T_c. The (100) and (110) junctions are the same ones as shown in Fig. 1. Curves are shifted vertically in (a), (b), (d), and (e) for clarity. (g) - (i) Peak position, V_p ((filled green circles), and steepest slope point, V_s (filled black squares), of the FIG at low temperature (Ref. 33, Sect. 9). In (g) & (h),

Δ is also plotted for $H = 0.2$ T with (Δ, Γ, Z) = (0.69 meV, 0.405 meV, 1.81) for (g) and (0.535 meV, 0.198 meV, 1.21) for (h). The crossing field (H_c) is indicated by gray lines. In (h), slope-changing points due to the pairing gap, V_{ps}, above H_c are also shown by filled triangles. Dash-dotted and dashed lines are linear fits to V_p and V_s, respectively. The blue dotted lines crossing the point Δ(0.2 T) in (g) and (h) show field dependence of the pairing gap according to the GL theory (see the text).

Fig. 5. Absence of the FIG above T_p. Magnetic field dependence of the high-bias normalized conductance for a (001) junction on $CeCoIn_5$ at (a) T = 10 K and (b) T = 15 K. The broad peak at zero bias is suppressed gradually with increasing magnetic field, merging into the background without the FIG feature. Insets: G_b curves showing a very small change with the field. The faint gaplike feature appearing at high field (zero-bias conductance depth smaller than 0.5% for 14 T) is unlikely to be intrinsic as it depends on the background normalization, e.g., the bias range taken for the quasi-linear background conductance.

Fig. 6. Comparison of the FIG in $CeCoIn_5$ with calculation based on the Anderson-Appelbaum (AA) theory. (a) & (b), Experimental G_b curves for the (100) and (110) junctions, respectively, taken at 20 mK and two fields in the high field limit where the FIG is most pronounced. (c) G_n curves calculated based on the AA theory for the same fields and temperature as in (1) & (b). The expressions for G_2 (spin flip inelastic tunneling) and G_3 (Kondo resonant tunneling) terms are adopted from Ref. 61 with the weight factor of 0.5 per each. The g-factor is 2 and the spin is 1/2. The vertical gray lines indicate the bias voltages corresponding to $\pm E_Z$ at $H = 18$ T.

REFERENCES

[1] W. K. Park, J. L. Sarrao, J. D. Thompson, and L. H. Greene, *Andreev reflection in heavy-fermion superconductors and order parameter symmetry in* $CeCoIn_5$, Phys. Rev. Lett. **100**, 177001 (2008).

[2] J. D. Thompson and Z. Fisk, *Progress in Heavy-Fermion Superconductivity: Ce115 and Related Materials*, J. Phys. Soc. Jpn. **81**, 011002 (2012).

[3] D. J. Scalapino, *A common thread: The pairing interaction for unconventional superconductors*, Rev. Mod. Phys. **84**, 1383 (2012).

[4] M. T. Béal-Monod, C. Bourbonnais, and V. J. Emery, *Possible superconductivity in nearly antiferromagnetic itinerant fermion systems*, Phys. Rev. B **34**, 7716 (1986).

[5] K. Miyake, S. Schmittrink, and C. M. Varma, *Spin-Fluctuation-Mediated Even-Parity Pairing in Heavy-Fermion Superconductors*, Phys. Rev. B **34**, 6554 (1986).

[6] D. J. Scalapino, E. Loh, and J. E. Hirsch, *D-Wave Pairing near a Spin-Density-Wave Instability*, Phys. Rev. B **34**, 8190 (1986).

[7] J. F. Zasadzinski, L. Ozyuzer, N. Miyakawa, K. E. Gray, D. G. Hinks, and C. Kendziora, *Correlation of tunneling spectra in* $Bi_2Sr_2CaCu_2O_{8+\delta}$ *with the resonance spin excitation*, Phys. Rev. Lett. **87**, 067005 (2001).

[8] F. C. Niestemski, S. Kunwar, S. Zhou, S. L. Li, H. Ding, Z. Q. Wang, P. C. Dai, and V. Madhavan, *A distinct bosonic mode in an electron-doped high-transition-temperature superconductor*, Nature **450**, 1058 (2007).

[9] S. Chi *et al.*, *Imaging the real space structure of the spin fluctuations in an iron-based superconductor*, Nat. Commun. **8**, 15996 (2017).

[10] S. D. Wilson, P. C. Dai, S. L. Li, S. X. Chi, H. J. Kang, and J. W. Lynn, *Resonance in the electron-doped high-transition-temperature superconductor* $Pr_{0.88}LaCe_{0.12}CuO_{4-\delta}$, Nature **442**, 59 (2006).

[11] A. D. Christianson *et al.*, *Unconventional superconductivity in* $Ba_{0.6}K_{0.4}Fe_2As_2$ *from inelastic neutron scattering*, Nature **456**, 930 (2008).

[12] J. M. Rowell, P. W. Anderson, and D. E. Thomas, *Image of the Phonon Spectrum in the Tunneling Characteristic Between Superconductors*, Phys. Rev. Lett. **10**, 334 (1963).

[13] J. R. Schrieffer, D. J. Scalapino, and J. W. Wilkins, *Effective Tunneling Density of States in Superconductors*, Phys. Rev. Lett. **10**, 336 (1963).

[14] J. C. Swihart, D. J. Scalapino, and Y. Wada, *Solution of Gap Equation for Pb Hg and Al*, Phys. Rev. Lett. **14**, 106 (1965).

[15] W. L. McMillan and J. M. Rowell, *Lead phonon spectrum calculated from superconducting density of states*, Phys. Rev. Lett. **14**, 108 (1965).

[16] C. Stock, C. Broholm, J. Hudis, H. J. Kang, and C. Petrovic, *Spin resonance in the d-wave superconductor* $CeCoIn_5$, Phys. Rev. Lett. **100**, 087001 (2008).

[17] A. V. Chubukov and L. P. Gor'kov, *Spin resonance in three-dimensional superconductors: The case of* $CeCoIn_5$, Phys. Rev. Lett. **101**, 147004 (2008).

[18] Y. Song *et al.*, *Robust upward dispersion of the neutron spin resonance in the heavy fermion superconductor* $Ce_{1-x}Yb_xCoIn_5$, Nat. Commun. **7**, 12774 (2016).

[19] S. Ernst, S. Wirth, F. Steglich, Z. Fisk, J. L. Sarrao, and J. D. Thompson, *Scanning tunneling microscopy studies on* $CeCoIn_5$ *and* $CeIrIn_5$, Phys. Status Solidi B **247**, 624 (2010).

[20] Y. Fasano, P. Szabo, J. Kacmarcik, Z. Pribulova, P. Pedrazzini, P. Samuely, and V. F. Correa, *Unconventional superconductivity in the strong-coupling limit for the heavy fermion system* $CeCoIn_5$, Physica B **536**, 798 (2018).

[21] A. Gyenis, B. E. Feldman, M. T. Randeria, G. A. Peterson, E. D. Bauer, P. Aynajian, and A. Yazdani, *Visualizing heavy fermion confinement and Pauli-limited superconductivity in layered* $CeCoIn_5$, Nat. Commun. **9**, 549 (2018).

[22] M. P. Allan, F. Massee, D. K. Morr, J. Van Dyke, A. W. Rost, A. P. Mackenzie, C. Petrovic, and J. C. Davis, *Imaging Cooper pairing of heavy fermions in* $CeCoIn_5$, Nat. Phys. **9**, 468 (2013).

[23] B. B. Zhou, S. Misra, E. H. D. Neto, P. Aynajian, R. E. Baumbach, J. D. Thompson, E. D. Bauer, and A. Yazdani, *Visualizing nodal heavy fermion superconductivity in* $CeCoIn_5$, Nat. Phys. **9**, 474 (2013).

[24] C. Petrovic, P. G. Pagliuso, M. F. Hundley, R. Movshovich, J. L. Sarrao, J. D. Thompson, Z. Fisk, and P. Monthoux, *Heavy-fermion superconductivity in* $CeCoIn_5$ *at 2.3 K*, J. Phys.: Condens. Matter **13**, L337 (2001).

[25] R. Flint, M. Dzero, and P. Coleman, *Heavy electrons and the symplectic symmetry of spin*, Nat. Phys. **4**, 643 (2008).

[26] R. Flint and P. Coleman, *Tandem Pairing in Heavy-Fermion Superconductors,* Phys. Rev. Lett. **105**, 246404 (2010).

[27] D. L. Cox and M. Jarrell, *The two-channel Kondo route to non-Fermi-liquid metals*, J. Phys.: Condens. Matter **8**, 9825 (1996).

[28] M. Jarrell, H. B. Pang, and D. L. Cox, *Phase diagram of the two-channel Kondo lattice*, Phys. Rev. Lett. **78**, 1996 (1997).

[29] P. Coleman, A. M. Tsvelik, N. Andrei, and H. Y. Kee, *Co-operative two-channel Kondo effect*, J. Phys.: Condens. Matter **10**, L239 (1998).

[30] W. K. Park, L. Sun, A. Noddings, D.-J. Kim, Z. Fisk, and L. H. Greene, *Topological surface states interacting with bulk excitations in the Kondo insulator* SmB_6 *revealed via planar tunneling spectroscopy* Proc. Natl. Acad. Sci. U. S. A. **113**, 6599 (2016).

[31] A. Bianchi, R. Movshovich, C. Capan, P. G. Pagliuso, and J. L. Sarrao, *Possible Fulde-Ferrell-Larkin-Ovchinnikov superconducting state in* $CeCoIn_5$, Phys. Rev. Lett. **91**, 187004 (2003).

[32] H. A. Radovan, N. A. Fortune, T. P. Murphy, S. T. Hannahs, E. C. Palm, S. W. Tozer, and D. Hall, *Magnetic enhancement of superconductivity from electron spin domains*, Nature **425**, 51 (2003).

[33] Y. Matsuda and H. Shimahara, *Fulde-Ferrell-Larkin-Ovchinnikov state in heavy fermion superconductors*, J. Phys. Soc. Jpn. **76**, 051005 (2007).

[34] M. Kenzelmann *et al.*, *Coupled superconducting and magnetic order in* $CeCoIn_5$, Science **321**, 1652 (2008).

[35] M. Kenzelmann *et al.*, *Evidence for a Magnetically Driven Superconducting Q Phase of* $CeCoIn_5$, Phys. Rev. Lett. **104**, 127001 (2010).

[36] D. Y. Kim, S. Z. Lin, F. Weickert, M. Kenzelmann, E. D. Bauer, F. Ronning, J. D. Thompson, and R. Movshovich, *Intertwined Orders in Heavy-Fermion Superconductor* $CeCoIn_5$, Phys. Rev. X **6**, 041059 (2016).

[37] V. S. Zapf, E. J. Freeman, E. D. Bauer, J. Petricka, C. Sirvent, N. A. Frederick, R. P. Dickey, and M. B. Maple, *Coexistence of superconductivity and antiferromagnetism in* $CeRh_{1-x}Co_xIn_5$, Phys. Rev. B **65**, 014506 (2002).

[38] W. K. Park, L. H. Greene, J. L. Sarrao, and J. D. Thompson, *Andreev reflection spectroscopy of the heavy-fermion superconductor* $CeCoIn_5$ *along three different crystallographic orientations*, Physica C (Amsterdam) **460**, 206 (2007).

[39] See Supplemental Material at [URL will be inserted by publisher] for detailed information.

[40] G. E. Blonder, M. Tinkham, and T. M. Klapwijk, *Transition from metallic to tunneling regimes in superconducting microconstrictions: excess current, charge imbalance, and supercurrent conversion*, Phys. Rev. B **25**, 4515 (1982).

[41] S. Kashiwaya, Y. Tanaka, M. Koyanagi, and K. Kajimura, *Theory for tunneling spectroscopy of anisotropic superconductors*, Phys. Rev. B **53**, 2667 (1996).

[42] C. R. Hu, *Midgap Surface-States as a Novel Signature for* d_{x2-y2}*-Wave Superconductivity*, Phys. Rev. Lett. **72**, 1526 (1994).

[43] M. Covington, M. Aprili, E. Paraoanu, L. H. Greene, F. Xu, J. Zhu, and C. A. Mirkin, *Observation of surface-induced broken time-reversal symmetry in* $YBa_2Cu_3O_7$ *tunnel junctions*, Phys. Rev. Lett. **79**, 277 (1997).

[44] T. Lofwander, V. S. Shumeiko, and G. Wendin, *Andreev bound states in high-*T_c *superconducting junctions*, Supercond. Sci. Technol. **14**, R53 (2001).

[45] G. Deutscher, *Andreev-Saint-James reflections: A probe of cuprate superconductors*, Rev. Mod. Phys. **77**, 109 (2005).

[46] H. O. Frota, *Shape of the Kondo Resonance*, Phys. Rev. B **45**, 1096 (1992).

[47] M. Aprili, E. Badica, and L. H. Greene, *Doppler shift of the Andreev bound states at the YBCO surface*, Phys. Rev. Lett. **83**, 4630 (1999).

[48] G. Deutscher, *Andreev-Saint James reflections as a tool for the study of unconventional superconductors*, New Challenges in Superconductivity: Experimental Advances and Emerging Theories **183**, 37 (2005).

[49] V. A. Sidorov, M. Nicklas, P. G. Pagliuso, J. L. Sarrao, Y. Bang, A. V. Balatsky, and J. D. Thompson, *Superconductivity and quantum criticality in* $CeCoIn_5$, Phys. Rev. Lett. **89**, 157004 (2002).

[50] K. Izawa, H. Yamaguchi, Y. Matsuda, H. Shishido, R. Settai, and Y. Onuki, *Angular position of nodes in the superconducting gap of quasi-2D heavy-fermion superconductor* $CeCoIn_5$, Phys. Rev. Lett. **87**, 057002 (2001).

[51] K. K. Gomes, A. N. Pasupathy, A. Pushp, S. Ono, Y. Ando, and A. Yazdani, *Visualizing pair formation on the atomic scale in the high-*T_c *superconductor* $Bi_2Sr_2CaCu_2O_{8+\delta}$, Nature **447**, 569 (2007).

[52] T. Kondo, Y. Hamaya, A. D. Palczewski, T. Takeuchi, J. S. Wen, Z. J. Xu, G. D. Gu, J. Schmalian, and A. Kaminski, *Disentangling Cooper-pair formation above the transition temperature from the pseudogap state in the cuprates*, Nat. Phys. **7**, 21 (2011).

[53] H. Y. Choi, Y. Y. Bang, and D. K. Campbell, *Andreev reflections in the pseudogap state of cuprate superconductors*, Phys. Rev. B **61**, 9748 (2000).

[54] M. Maltseva, M. Dzero, and P. Coleman, *Electron cotunneling into a Kondo lattice*, Phys. Rev. Lett. **103**, 206402 (2009).

[55] J. Figgins and D. K. Morr, *Differential conductance and quantum interference in Kondo systems*, Phys. Rev. Lett. **104**, 187202 (2010).

[56] P. Wölfle, Y. Dubi, and A. V. Balatsky, *Tunneling into clean heavy fermion compounds: origin of the Fano line shape*, Phys. Rev. Lett. **105**, 246401 (2010).

[57] M. Fogelström, W. K. Park, L. H. Greene, G. Goll, and M. J. Graf, *Point-contact spectroscopy in heavy-fermion superconductors*, Phys. Rev. B **82**, 014527 (2010).

[58] W. K. Park, P. H. Tobash, F. Ronning, E. D. Bauer, J. L. Sarrao, J. D. Thompson, and L. H. Greene, *Observation of the hybridization gap and Fano resonance in the Kondo lattice* URu_2Si_2, Phys. Rev. Lett. **108**, 246403 (2012).

[59] M. Sundermann *et al.*, *Orientation of the ground-state orbital in* $CeCoIn_5$ *and* $CeRhIn_5$, Phys. Rev. B **99**, 235143 (2019).

[60] T. J. Reber *et al.*, Pairing, pair-breaking, and their roles in setting the T_c of cuprate high temperature superconductors, arXiv:1508.06252 (2015).

[61] L. Y. L. Shen and J. M. Rowell, *Zero-Bias Tunneling Anomalies - Temperature, Voltage, and Magnetic Field Dependence*, Phys. Rev. **165**, 566 (1968).

[62] D. L. Losee and E. L. Wolf, *Tunneling Spectroscopy of Cds Schottky Barrier Junctions*, B Am Phys Soc **14**, 736 (1969).

[63] Y. H. Zhang, S. Kahle, T. Herden, C. Stroh, M. Mayor, U. Schlickum, M. Ternes, P. Wahl, and K. Kern, *Temperature and magnetic field dependence of a Kondo system in the weak coupling regime*, Nat. Commun. **4**, 2110 (2013).

[64] P. W. Anderson, *Localized Magnetic States and Fermi-Surface Anomalies in Tunneling*, Phys. Rev. Lett. **17**, 95 (1966).

[65] J. Appelbaum, *s-d Exchange Model of Zero-Bias Tunneling Anomalies*, Phys. Rev. Lett. **17**, 91 (1966).

[66] L. Sun, D. J. Kim, Z. Fisk, and W. K. Park, *Planar tunneling spectroscopy of the topological Kondo insulator* SmB_6, Phys. Rev. B **95**, 195129 (2017). We also note that such a ZBCP (or more broadly called, zero-bias anomaly (ZBA)) has never been observed in our standard junctions such as Al/AlO_x/Pb and Nb/AlO_x/Ag or Pb prepared under the same conditions as for the $CeCoIn_5$/AlO_x/Pb junctions. According to Ref. 61, such a ZBA was observed mostly in junctions prepared under abnormal conditions. Thus, all things considered, the AlO_x barrier formed in normal conditions (thermal or plasma oxidation at room temperature of a deposited Al film) is not likely to produce Kondo-like moments.

[67] A. Sundaresan, R. Bhargavi, N. Rangarajan, U. Siddesh, and C. N. R. Rao, *Ferromagnetism as a universal feature of nanoparticles of the otherwise nonmagnetic oxides*, Phys. Rev. B **74**, 161306 (2006).

[68] A. G. M. Jansen, A. P. Vangelder, and P. Wyder, *Point-contact spectroscopy in metals*, J. Phys. C **13**, 6073 (1980).

[69] W. K. Park and L. H. Greene, *Andreev reflection and order parameter symmetry in heavy-fermion superconductors: the case of* $CeCoIn_5$, J. Phys.: Condens. Matter **21**, 103203 (2009).

[70] K. Nagaoka, T. Jamneala, M. Grobis, and M. F. Crommie, *Temperature dependence of a single Kondo impurity*, Phys. Rev. Lett. **88**, 077205 (2002).

[71] D. H. Douglass, *Magnetic Field Dependence of Superconducting Penetration Depth in Thin Specimens*, Phys. Rev. **124**, 735 (1961).

[72] C. Stock, C. Broholm, Y. Zhao, F. Demmel, H. J. Kang, K. C. Rule, and C. Petrovic, *Magnetic Field Splitting of the Spin Resonance in* $CeCoIn_5$, Phys. Rev. Lett. **109**, 167207 (2012).

[73] H. Won, K. Maki, S. Haas, N. Oeschler, F. Weickert, and P. Gegenwart, *Upper critical field and Fulde-Ferrell-Larkin-Ovchinnikov state in* $CeCoIn_5$, Phys. Rev. B **69**, 180504 (2004).

[74] A. Bianchi, R. Movshovich, N. Oeschler, P. Gegenwart, F. Steglich, J. D. Thompson, P. G. Pagliuso, and J. L. Sarrao, *First-order superconducting phase transition in CeCoIn*$_5$, Phys. Rev. Lett. **89**, 137002 (2002).

[75] J. S. Van Dyke, F. Massee, M. P. Allan, J. C. S. Davis, C. Petrovic, and D. K. Morr, *Direct evidence for a magnetic f-electron-mediated pairing mechanism of heavy-fermion superconductivity in CeCoIn*$_5$, Proc. Natl. Acad. Sci. U. S. A. **111**, 11663 (2014).

[76] H. Kim, M. A. Tanatar, R. Flint, C. Petrovic, R. Hu, B. D. White, I. K. Lum, M. B. Maple, and R. Prozorov, *Nodal to Nodeless Superconducting Energy-Gap Structure Change Concomitant with Fermi-Surface Reconstruction in the Heavy-Fermion Compound CeCoIn*$_5$, Phys. Rev. Lett. **114**, 027003 (2015).

[77] O. Erten, R. Flint, and P. Coleman, *Molecular Pairing and Fully Gapped Superconductivity in Yb-doped CeCoIn*$_5$, Phys. Rev. Lett. **114**, 027002 (2015).

[78] S. Nakatsuji, S. Yeo, L. Balicas, Z. Fisk, P. Schlottmann, P. G. Pagliuso, N. O. Moreno, J. L. Sarrao, and J. D. Thompson, *Intersite Coupling Effects in a Kondo Lattice*, Phys. Rev. Lett. **89**, 106402 (2002).

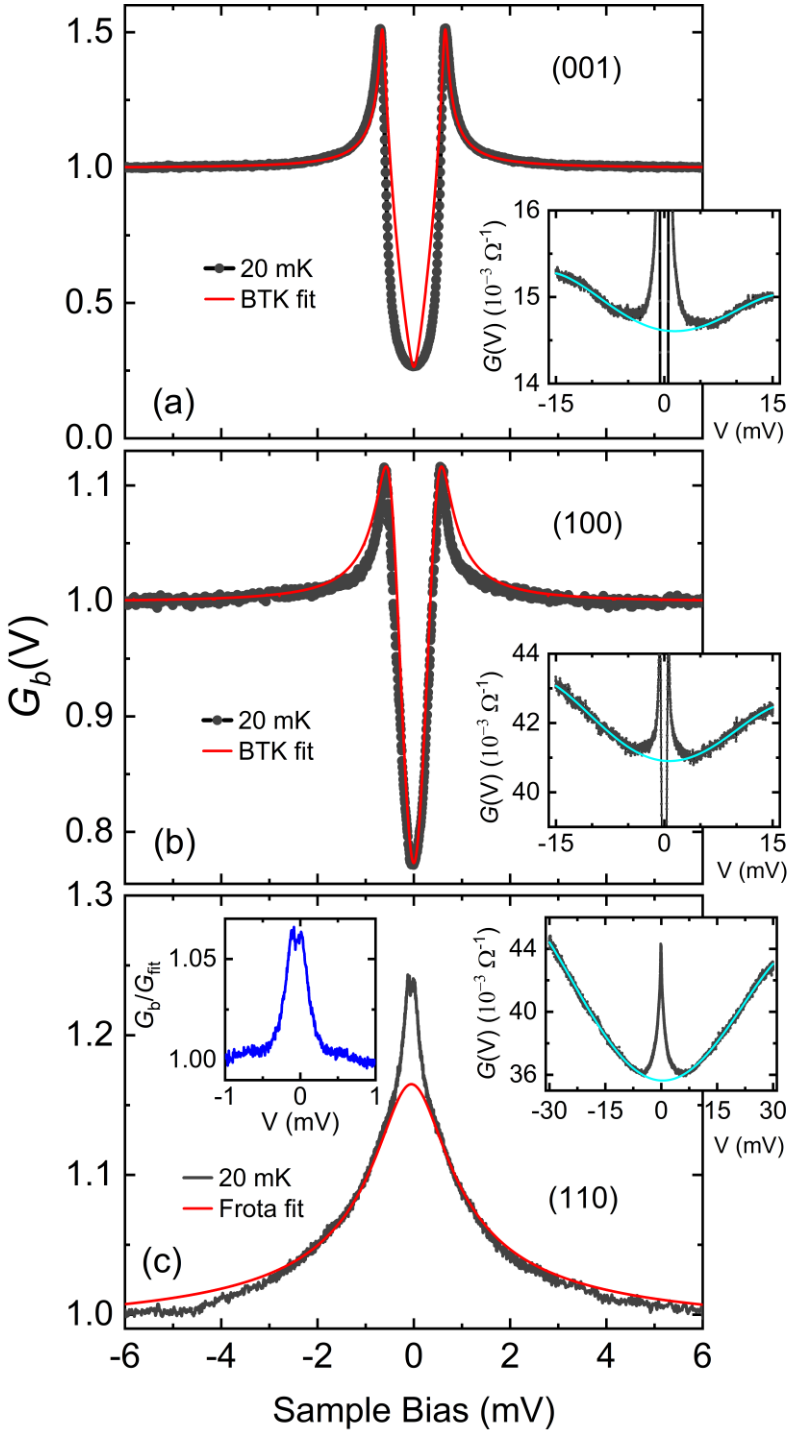

Figure 1, K. Shrestha et al.

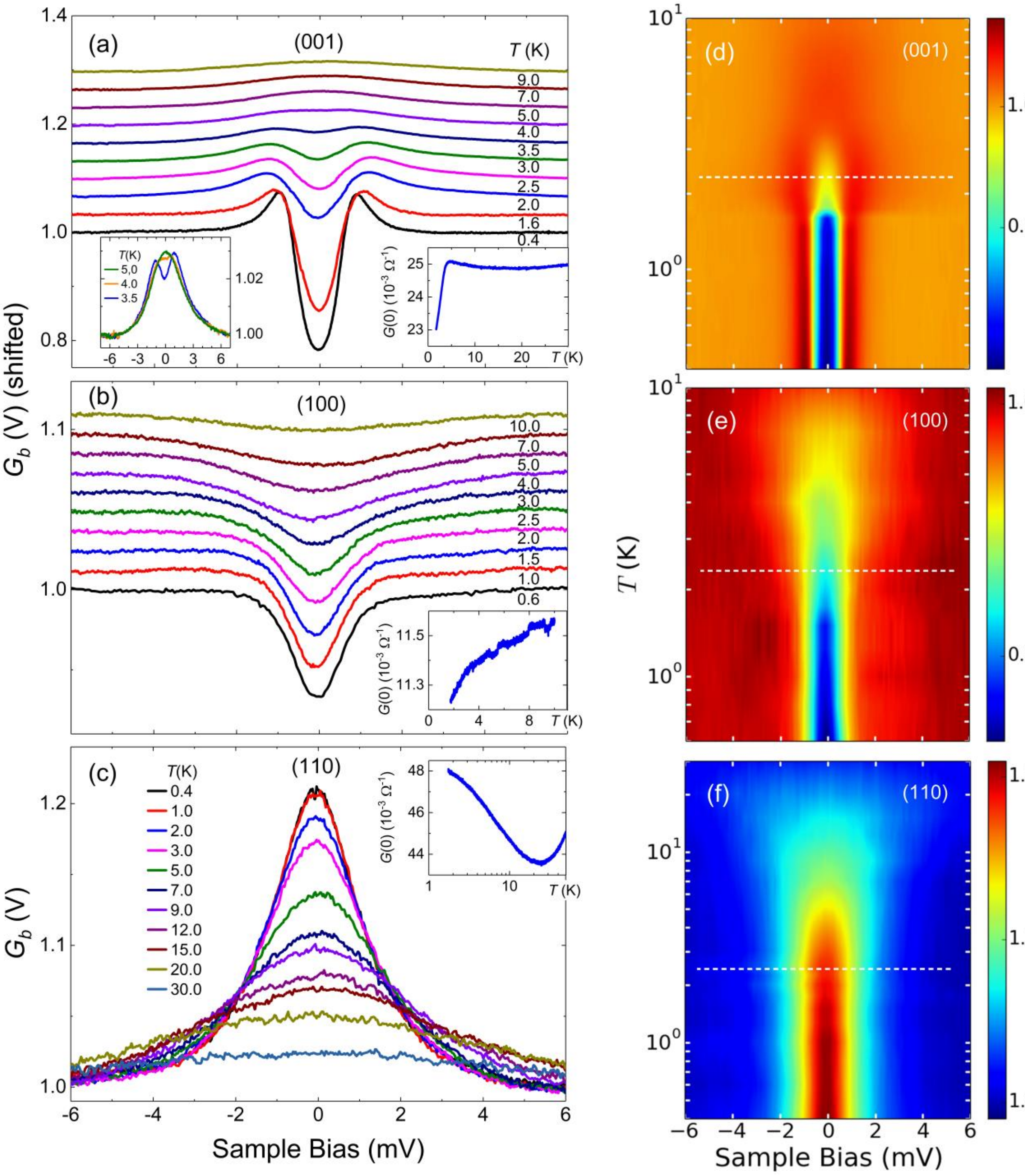

Figure 2, K. Shrestha et al.

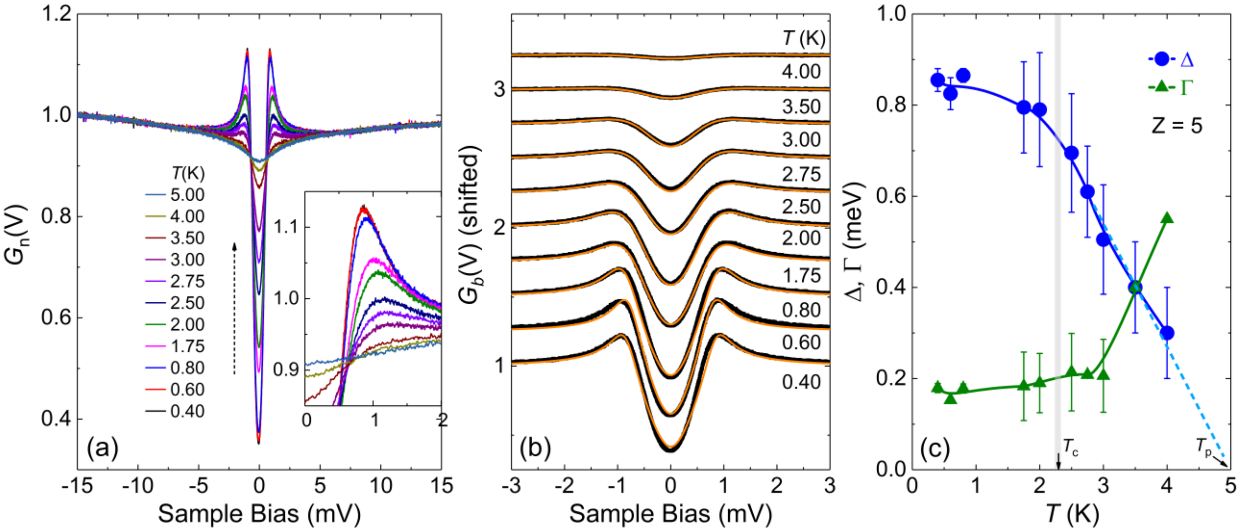

Figure 3, K. Shrestha et al.

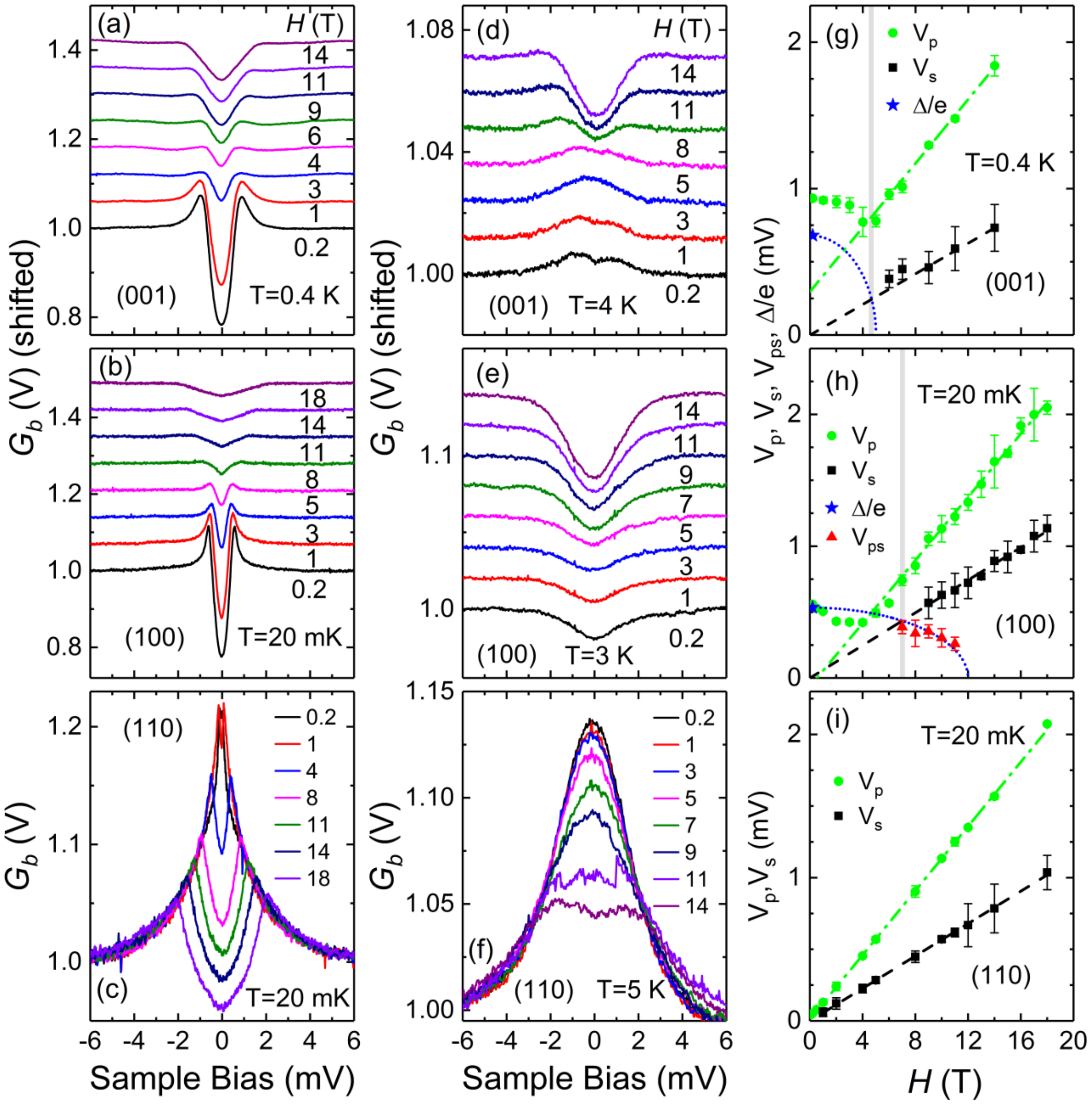

Figure 4, K. Shrestha et al.

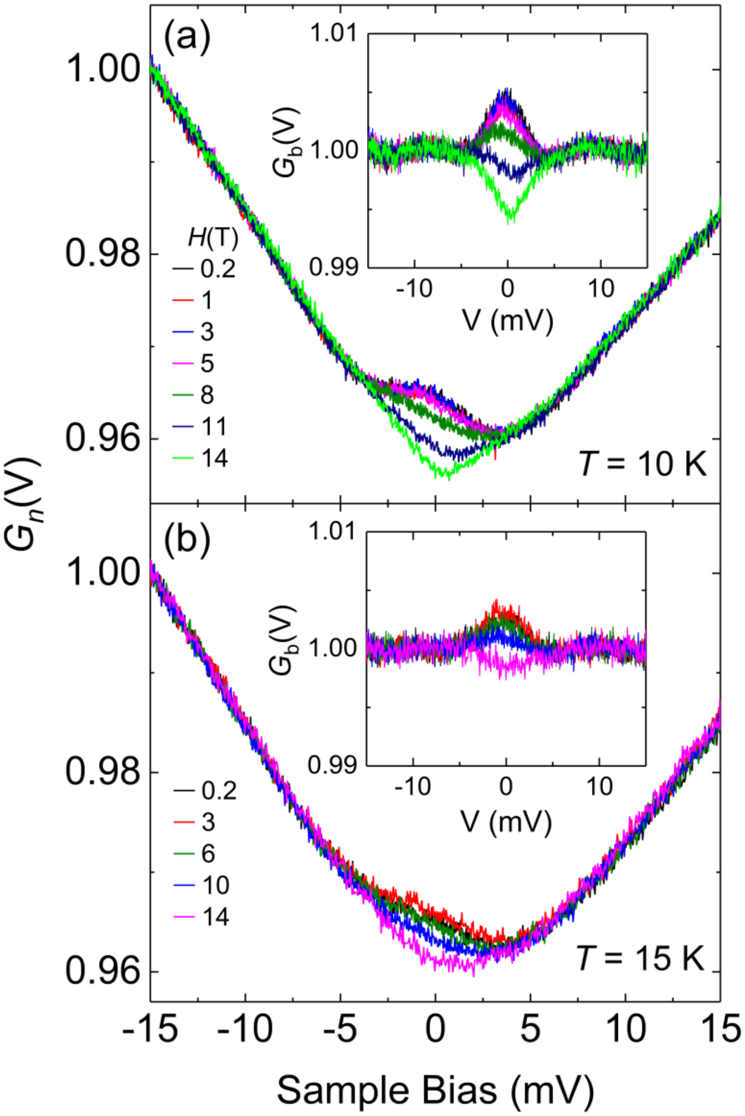

Figure 5, K. Shrestha et al.

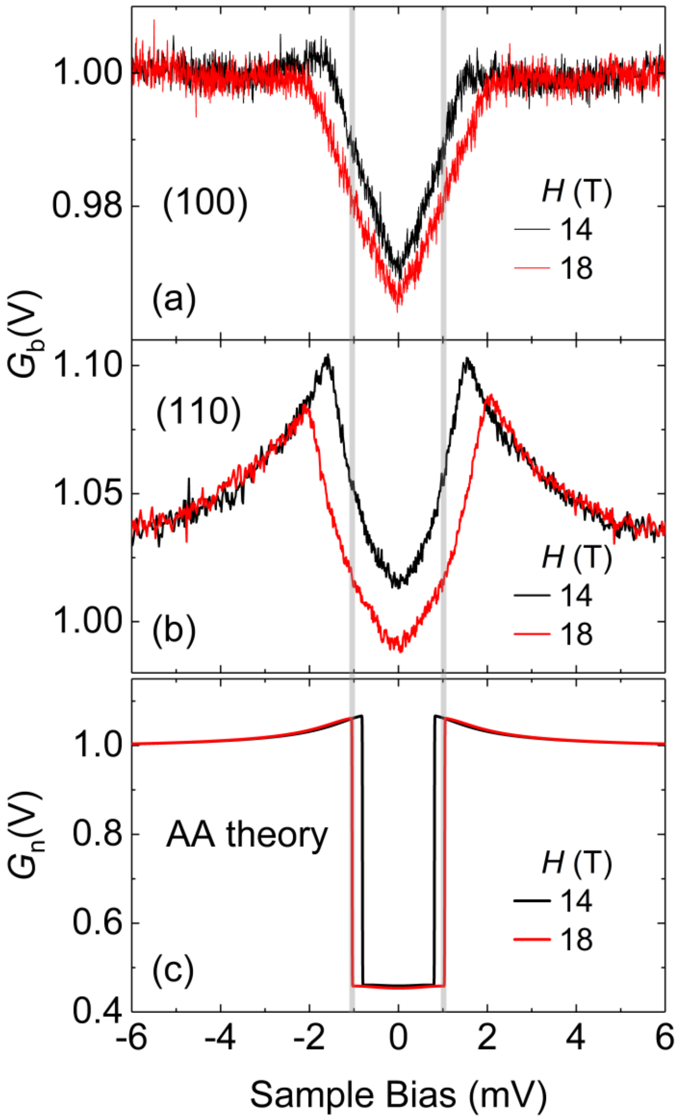

Figure 6, K. Shrestha et al.